COASTAL ENGINEERING JOURNAL
2018, VOL. 60, NO. 4, 423–436
https://doi.org/10.1080/21664250.2018.1498211

ORIGINAL RESEARCH PAPER

CFD modeling of tidal bores: development and validation challenges

Xinqian Leng [a], Bruno Simon [a,b,c], Nazanin Khezri[a,d], Pierre Lubin [b] and Hubert Chanson [a,b]

[a]School of Civil Engineering, The University of Queensland, Brisbane, Australia; [b]Université de Bordeaux, I2M, Laboratoire TREFLE, Pessac, France; [c]Aix-Marseille University, IRPHE, Marseille, France; [d]GHD, Brisbane, Australia

ABSTRACT

A tidal bore is a natural estuarine phenomenon forming a positive surge in a funnel-shaped river mouth during the early flood tide under spring tide conditions and low freshwater levels. The bore passage may induce some enhanced turbulent mixing, with upstream advection of suspended material. Herein, the flow field and turbulence characteristics of tidal bores were measured using both numerical computational fluid dynamics (CFD) and physical modeling. This joint modeling approach, combined with some theoretical knowledge, led to some new understanding of turbulent velocity field, turbulent mixing process, Reynolds stress tensor, and tidal bore hydrodynamics. Thétis is a CFD model using the volume of fluid technique to model the free-surface and Large Eddy Simulation (LES) technique for the turbulence modeling. Physical data sets were used to map the velocity and pressure field and resolve some unusual feature of the unsteady flow motion. A discussion will be provided to explain why a detailed validation process, involving a physical knowledge of the flow, is crucial. Comparison of the numerical model results and experimental data over broad ranges of conditions for the same flow is mandatory. The validation process from two-dimensional to three-dimensional will be commented and difficulties will be highlighted.

ARTICLE HISTORY
Received 24 November 2017
Accepted 23 June 2018

KEYWORDS
Tidal bores; computational fluid dynamics (CFD); numerical modeling; validation processes; physical experiments

1. Introduction

A tidal bore is a positive surge occurring naturally during spring tide with large tidal range forming in a funnel-shaped river mouth and propagating upstream (Figure 1). Figure 1 presents photographs of tidal bores in France and China (Left) and of tidal bores in a relatively large-size laboratory facility (19 m long, 0.7 m wide) (Left). The tidal bore induces enhanced turbulent mixing and a large amount of sediment load during its inland propagation. Laboratory observations and computational fluid dynamics (CFD) calculations highlighted a number of seminal features of tidal bore investigations. Several common features were observed. First, a tidal bore is a positive surge, a compression wave, and a hydraulic jump in translation (Lighthill, 1978; Lubin and Chanson, 2017). It is a hydrodynamic shock, with no net mass flux, i.e. it is not a periodic wave. A tidal bore is an unsteady, highly turbulent flow motion. The shape of the tidal bore is governed by its Froude number, defined as $Fr = (V_1 + U)/(g \times A_1/B_1)^{1/2}$, where V_1 is the initial velocity positive downstream, U is the bore celerity positive upstream, g is the gravity acceleration, A_1 is the initial cross-sectional area and B_1 is the initial free-surface width (Chanson, 2012). In a rectangular channel, the bore Froude number equals $Fr = (V_1 + U)/(g \times d_1)^{1/2}$ with d_1 the initial flow depth. For an undular non-breaking bore, $Fr < 1.2$–1.3 (Peregrine, 1966; CHANSON, 2010), while $Fr > 1.5$–1.8 for a breaking bore. An undular bore with some breaking (also called breaking bore with secondary waves) is observed for an intermediate range of Froude numbers. For a breaking bore, the bore celerity is not truly constant; rather, it constantly fluctuates about a mean value (Leng and Chanson, 2015a). The fluctuations in bore celerity are large in both transverse and longitudinal directions, with ratio of standard deviation to mean value greater than unity. The bore roller toe perimeter constantly fluctuates with time and space, so it is not a straight line (Chanson, 2016; Wang, Leng, and Chanson, 2017).

A breaking tidal bore is a tri-phase flow, with three distinct phases flowing: liquid (water), solid (sediment), and gas (air) (Chanson, 2013; Leng and Chanson, 2015b). The three-phase nature of tidal bore flow was never accounted for, although it has been reported by numerous photographs and illustrations. In most tidal bore occurrences, the sediment load is large and turbulent modulation in sediment-laden flows must be significant (Figure 1B, Left). Suspended sediment concentrations in excess of 20 kg/m^3 were observed in the field (Garonne, Sélune, Sée, Qiantang Rivers). For such large-suspended sediment loads, and together with rheological data (Faas, 1995; Chanson et al., 2011; Keevil, Chanson, and Reungoat, 2015), a non-Newtonian flow behavior could be expected, i.e. typically a non-Newtonian thixiotropic flow. To date, the non-Newtonian behavior of sediment-laden tidal bore flow was never considered nor

CONTACT Pierre Lubin pierre.lubin@enscbp.fr

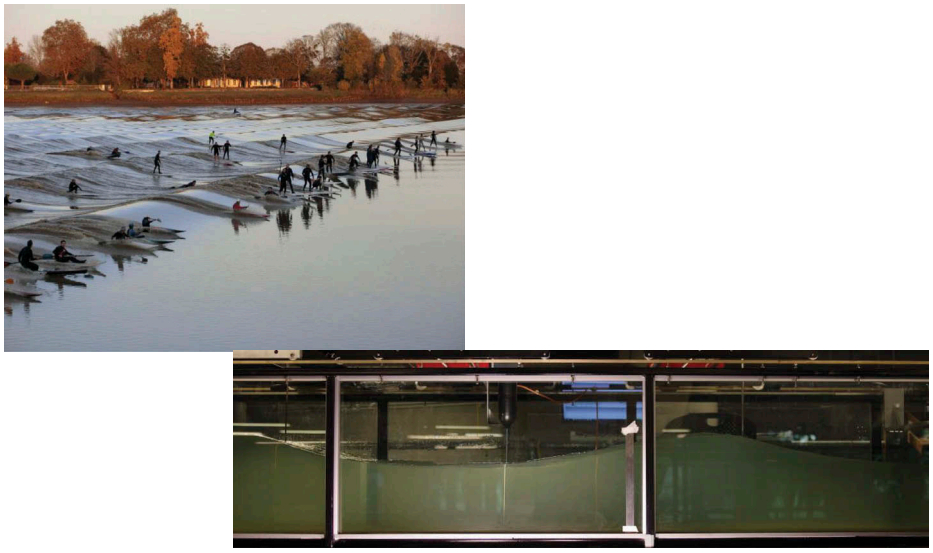

(A) Undular bores - (Left) Undular bore of the Dordogne River bore at Saint Pardon (France) on 30 October 2015, propagating from left to right; (Right) Laboratory undular bore (Fr = 1.2) propagating from left to right

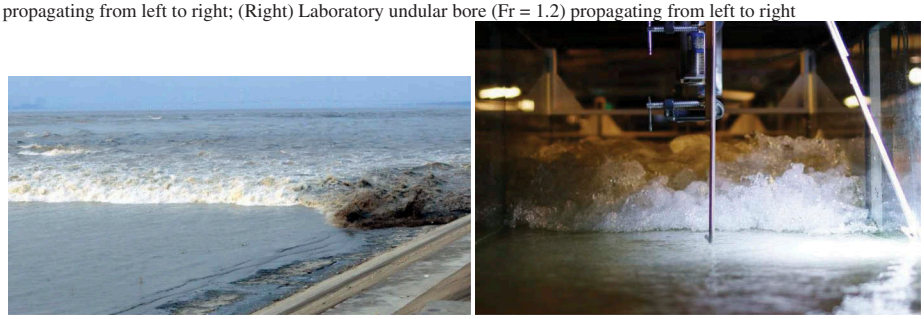

(B) Breaking bores - (Left) Qiantang River bore at Meilvba (China) on 22 September 2016, propagating from top right to bottom left; (Right) Looking downstream at incoming breaking bore (Fr = 2.2) in laboratory

Figure 1. Photographs of tidal bores in the field (Left) and in laboratory (Right).

modeled, and no study was undertaken in three-phase flows with high sediment and air content despite the high practical relevance.

A tidal bore is technically a hydraulic jump in translation (Chanson, 2009). There are analogies between stationary hydraulic jumps, positive surges, compression waves, and estuarine bores (tidal bores, tsunami bores) as discussed recently (Wang, Leng, and Chanson, 2017; Lubin and Chanson, 2017). In the present contribution, we wish to focus on tidal bore propagation in natural channel. The literature on positive surges in hydropower canals is relevant, albeit validation of numerical modeling is restricted by the very limited number of field data sets, mostly free-surface observations (e.g. Cunge, 1966; 1967).

Historically, numerical modeling of positive surges and tidal bores was based upon one-dimensional and two-dimensional (2D) depth-averaged models (Preissmann and Cunge, 1967; Madsen, Simonsen, and Pan, 2005). Since 2009, CFD modeling of tidal bore flows was conducted at the University of Bordeaux, with detailed validation data sets obtained at the University of Queensland in large-size flumes. The aim of this paper is to present the latest CFD developments and validation results, as well as to discuss challenges associated with the validation process. It will be argued that a detailed validation process is crucial, and requires a solid expert knowledge of the physical processes.

2. CFD modeling developments

In the breaking bore simulation, the difficulties with free-surface modeling include significant air–water interactions at the free surface and numerical diffusion caused by large deformations of the air–water interface. Lubin, Glockner, and Chanson (2010a, 2010b) presented two dimensional numerical results, solving the Navier–Stokes equations in air and water, coupled with a subgrid scale turbulence model (Large Eddy Simulation – LES). The general trends of the flow behavior were observed: the bore front passage was shown to be associated with a rapid flow deceleration, coupled with a sudden increase in water depth. The numerical data were qualitatively in agreement with field and laboratory data. These encouraging preliminary results demonstrated the need for realistic inflow conditions, to be specified at the inlet boundary. Numerical simulations of 2D undular and

breaking bores in an open channel were performed by Khezri (2014) to investigate the characteristics of turbulent flow beneath the bores. Some unsteady two-phase tidal bore motion was simulated for further understanding of the tidal bore. The simulations were performed with flow conditions comparable to the experimental studies of Khezri (2014) (Table 1), and these experimental data were used to validate the CFD modeling. The flow characteristics were chosen to be similar to the experiments: the bore was generated through the sudden closure of a Tainter gate at the downstream end of the channel, and the bore traveled against an initially steady flow. The complete closure of the gate resulted in a breaking bore (Fr = 1.32–1.4) and the gate closure with partial opening underneath the gate produced an undular bore (Fr = 1–1.30). The pressure distribution measured beneath the breaking bore was comparable to experimental estimates. The vortical structures were mapped and visualized using the numerical data. The observation of coherent structures, and their upward motion beneath the breaking bore in the numerical study, could explain the observed upward particle motion observations during the breaking bore experiments. On another hand, when considering the free-surface and velocities evolutions, discrepancies were observed. The numerical modeling was conducted with the same inflow conditions and downstream/upstream boundary conditions as the physical experiments, in order to generate targeted breaking and undular bores. That is, the initial flow depth, depth-averaged velocity, and the gate opening after closure (for the undular case) were identical. With these conditions, the numerical modeling yielded slightly different tidal bore characteristics. It was acknowledged that the numerical and experimental modeling of undular bore did not show exactly similar characteristics, although the numerical simulation was configured based on the experimental modeling. The Froude number and bore celerity were found to be higher in the numerical simulation compared to the experimental modeling (Table 1). Table 1 compares some characteristics of undular bore in the experimental and numerical modeling. It was speculated that the differences could be explained by both experimental and numerical errors. It was also suggested that other differences between experimental and numerical modeling could be caused by the bore generation process. Indeed, the undular bore generation in the physical channel needed some mechanical trigger from downstream, which could have some effects on the bore characteristics. Ultimately, the flow characteristics were chosen with similar initial condition as experiments, the closest possibly, so the results were still comparable, as the numerical results showed similar trends as experimental results.

Table 1 Tidal bore flow conditions modeled by Khezri (2014) in a 0.5-m-width rectangular channel with rough bed.

Bore type	Model	Bore celerity U ($m.s^{-1}$)	Fr
Breaking	Physical	0.86	1.36
	Numerical (CFD)	1.01	1.53
Undular	Physical	0.63	1.17
	Numerical (CFD)	0.83	1.43

Chanson, Lubin, and Glockner (2012) discussed and proved a need for more realistic unsteady inflow conditions (Jarrin et al., 2006) to be specified at the inlet boundary. The three-dimensional (3D) numerical simulation of a weak breaking bore generation and propagation was presented for the first time. Some simulation time was first required for the injected turbulent boundary condition to propagate along the rectangular open channel. Then, the wall boundary condition was set at the left side of the numerical domain to mimic the experimental closing gate. In the breaking bore simulation, the difficulties with free-surface modeling include significant air–water interactions at the free surface and numerical diffusion caused by large deformations of the air–water interface.

Simon (2014) focused on 2D and 3D numerical simulations of undular bores, to investigate the characteristics of turbulent flow beneath the bores, considering partial and complete gate opening. The steady-flow turbulence was recreated by using a synthetic eddy method (SEM) on the domain inlet. The 3D undular bores were generated for the first time, analyzing the effect of an incoming turbulent river flow. The 3D free-surface evolution showed some characteristic bore features with the appearance of cross waves for the simulation realized with a bore Froude number of 1.26. The global evolution of bores was similar to experimental observations (CHANSON 2010). Depending on the bore generation method, the unsteady velocity data showed different evolution patterns. The simulations with a fully closed gate showed successive flow reversals beneath crests and troughs. The simulations with a partially closed gate showed velocity reversal zones close to the bed and sidewalls following the bore propagation. Close to the bed, the intensity of flow reversal reached maximum values of up to 1.7 and 0.9 times the initial steady-flow velocity for the case with a completely and partially closed gate, respectively. For the case with a gate partially closed, coherent structures were observed in the wake of the velocity reversals beneath the bore front close to the bed. In three dimensions, the flow generated complex structures. The coherent structures were advected downstream following the flow motion and tended to move upward in the water column, in agreement with qualitative experimental observations. The comparison of 2D and 3D simulations showed that the 2D simulations were insufficient to reproduce all the bores features, such as cross waves and coherent structures, but could give some basic results concerning the

global flow patterns. Nonetheless, the findings stressed the importance of studying the flow in three dimensions. The comparison of simulations with and without turbulence in the initial steady flow showed that the initial turbulence had a limited effect on the free-surface evolution and the bore celerity, but could have a more significant effect on the velocity field. Simon (2014) observed some limitation with the numerical simulation. The case with a partially closed gate presented some difference with earlier experimental results, as the initial steady-flow conditions between experiment and numerical simulation differed. These deviations were attributed to the mesh size selected upon the available computing resources. In the initially steady flow, some limitations also appeared with spurious velocities sometimes appearing next to the downstream boundary, which could sometimes disappear once the bore was generated. Nevertheless, the numerical work presented a simultaneous characterization of both the free surface and velocity, validated for each case with experimental data.

3. CFD model configuration for tidal bore simulations

3.1. Numerical model

New CFD modeling was conducted with a focus on 3D initially steady flow and 2D breaking bore simulations, over a relatively wide range of flow conditions. The finite volume method is used to discretize the system of equations. The interface tracking was achieved by applying the volume of fluid (VOF) technique. The VOF method is relatively simple and can be used to describe accurately the flow interface with rupture and reconnection. The basic idea is to locate the two media by a continuous color function C indicating the phase rate of presence, C = 0 for the air and C = 1 for the water. The function C depends on the fluid velocity and its evolution is described by an advection equation. No boundary condition is used between air and water; it is classically assumed that the free surface is located at C = 0.5. The governing equations, i.e. the Navier–Stokes equations and continuity equation, were discretized on a staggered grid with a finite-volume method. The implicit temporal discretization was utilized. The nonlinear convective terms were discretized by an upwind-centered scheme, whereas a second-order-centered scheme was chosen for the approximation of the viscous terms. The velocity/pressure coupling was performed with a pressure connection method. The method consists of two stages of velocity prediction and pressure correction in the Navier–Stokes system. The turbulence modeling was performed using LES technique. The free-surface tracking was achieved by VOF method to enable achieving the interface reconnections in the modeling of 2D two phase flows.

The code was parallelized using the MPI library. The linear system was solved using the HYPRE parallel solver and preconditioning library. A BICGStab solver (Bi-Conjugate Gradient Stabilized solver associated with a point Jacobi pre-conditioner) was used to solve the precondition steps and a GMRES solver (associated with a multi-grid pre-conditioner) for the correction steps. All the equations and details concerning the numerical tool are described by Lubin and Glockner (2015).

The 2D and 3D numerical domains were used in this study and partitioned into 24 subdomains (one processor per subdomain). For 2D models, the computation time was roughly 24–36 h. For 3D models, the computation time was 12–24 h for 2–4 s of flow. The simulation state was saved and stopped every 12–24 h to fit the supercomputer requirements. The simulations were continued about five times to get the presented physical times (at least 10 s).

3.2. Initial conditions

The 2D numerical domain was 12 m in the longitudinal (stream-wise) direction and 1 m in the vertical direction (Figure 2). A no-slip condition was imposed at the lower boundary (z = 0 m) and a Neumann condition was used at the upper boundary (z = 1 m). At the end of domain (x = 12 m), a wall boundary was imposed to act like a closed gate to reproduce the experimental generation process. The opening under the gate h_{out} could be set to introduce a Neumann condition between the bed (z = 0 m) and the bottom of the gate ($z = h_{out}$). For 2D models, the initial conditions were composed of a water trapezoid, with higher depth at inlet (d_{in}) to mimic the backwater effect in the physical gradually-varied flow. For 3D models, the depths at inlet and outlet were the same, i.e. a water rectangular cuboid. The initial and boundary parameters used in the 2D and 3D models were selected from experimental studies by Leng and Chanson (2016a).

The 3D model was built upon the 2D model configuration, by adding a third dimension being the transverse y dimension. The coordinate y was positive toward the left sidewall and the 3D numerical domain was 0.7 m wide. In this case, no-slip conditions were applied to both lateral walls and bottom of the domain. Table 2 documents detailed configurations of the 2D and 3D numerical models. In the table, S_o stands for the channel slope in the longitudinal direction. The opening under the gate after rapid closure is denoted h_{out}. Table 3 summarizes the experimental flow conditions corresponding to the three Froude numbers modeled in laboratory (Fr = 1.2, 1.5, 2.1). The reference depth d and celerity U were taken at the velocity sampling location, which was located

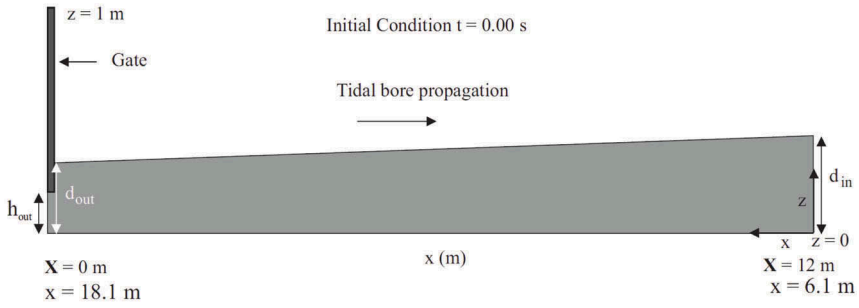

(A) Numerical domain configurations; X is the distance from the left boundary (i.e. gate) of the numerical domain; x is the distance from the upstream end of the physical channel

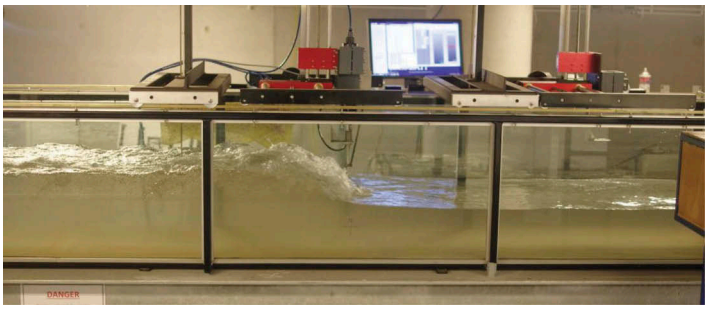

(B) Experiment in the 19 m long 0.7 m wide at the University of Queensland: Fr = 1.5, h_{out} = 0, S_o = 0

Figure 2. Definition sketch of numerical domain configurations and comparison with the physical model of Leng and Chanson (2016a, 2017a; b).

Table 2. Initial configuration of the 2D and 3D numerical simulations of tidal bores in a 0.7-m-width smooth channel.

Reference	Domain (m)	Mesh grid density	Fr	Q (m^3/s)	S_o	d_{in} (m)	d_{out} (m)	h_{out} (m)	Bore type
2D_Fr1.2	12 × 1	1600 × 100	1.2	0.101	0	0.208	0.19	0.071	Undular
2D_Fr1.5	12 × 1	2400 × 200	1.5	0.101	0	0.18	0.16	0	Breaking
2D_Fr2.1	12 × 1	1600 × 140	2.1	0.101	0.0075	0.1	0.1	0	Breaking
3D_Fr1.5	12 × 1 × 0.7	1600 × 250 × 200	1.5	0.101	0	0.17	0.17	0	Breaking
3D_Fr2.1	12 × 1 × 0.7	1600 × 250 × 200	2.1	0.101	0.0075	0.093	0.093	0	Breaking

Table 3. Flow conditions of the experimental data used to validate the numerical model (Leng and Chanson, 2016a).

Reference	Fr	Q (m^3/s)	S_o	d_1 (m)	U (m)	Bore type	Instrumentation
EA_Fr1.2	1.2	0.101	0	0.210	0.71	Undular	ADMs and ADV
EA_Fr1.5	1.5	0.101	0	0.180	1.13	Breaking	ADMs and ADV
EA_Fr2.1	2.1	0.101	0.0075	0.100	1.00	Breaking	ADMs and ADV

9.6 m upstream of the gate for both physical and numerical channels.

The 2D and 3D numerical domains are discretized into non-regular Cartesian cells. For numerical models denoted 2D_Fr1.2, in the longitudinal direction, the grid is clustered with a constant grid size Δx = 0.005 m from x = 0 to 4 m, then increasing exponentially for x = 4–12 m. In the vertical direction, the smallest mesh grid resolution Δz_{min} = 0.005 m is set at the bottom, while exponentially increasing between z = 0 and 0.1 m, then the grid is clustered with a constant grid size Δz = 0.005 m in the free-surface region (z = 0.1–0.5 m). An exponentially varied mesh was used above z = 0.5 m up to z = 1 m starting from a minimum Δz = 0.005 m.

For numerical models denoted 2D_Fr1.5, in the longitudinal direction, the grid is clustered with a constant grid size Δx = 0.005 m throughout the length of the numerical domain (x = 0–12 m). In the vertical direction, the grid is clustered with a constant grid size Δz = 0.005 m throughout the height of the numerical domain (z = 0–1 m).

For numerical models denoted 2D_Fr2.1, in the longitudinal direction, the grid is clustered with a constant grid size Δx = 0.005 m from x = 0 to 4 m, then increasing exponentially for x = 4–12 m. In the vertical direction, the smallest mesh grid resolution Δz_{min} = 0.005 m is set at the bottom, spacing constantly between z = 0 and 0.5 m, then the gird increased exponentially from z = 0.5 to 1 m with 50 grids.

For all 3D numerical models, in the longitudinal direction, the grid is clustered with a constant grid size Δx = 0.005 m from x = 0 to 4 m, then increasing exponentially for x = 4–12 m. In the vertical direction, the smallest mesh grid resolution Δz_{min} = 0.0025 m is set at the bottom, constantly spacing between z = 0 and 0.5 m, then exponentially increasing between z = 0.5 and 1 m with 50 grids. A constant spacing mesh was used in the transverse y direction throughout from y = 0–0.7 m with Δy = 0.0035 m.

4. Results

4.1. CFD simulation of the initially steady flow

During the physical experiments of tidal bores, the initially steady flow was left to run for at least 60 s before rapidly closing the downstream Tainter gate. A clear understanding of the flow physics and turbulent dynamics in the initially steady flow was essential as the tidal bores were very sensitive to the turbulent character of the inflow (Koch and Chanson, 2009; Chanson, Lubin, and Glockner, 2012). Past numerical CFD modeling on tidal bores included the works of Khezri (2014) and Simon (2014) provided limited to no information on the initially steady-flow properties before the bore arrival. As a result, the poor agreement in velocity fields between the 3D numerical simulation and experimental data could not be addressed due to the lack of validation in the steady-flow period. The present study expanded on previous works by simulating the initially steady flow before generating the bore for at least 10 s. The steady-flow characteristics simulated by the numerical CFD models were examined and compared to experimental results corresponding to the same flow conditions. The boundary layer properties and development were validated against physical experiments.

Herein, the inflow turbulence was generated using the SEM based on the view of turbulence as a superposition of coherent structures (Jarrin et al., 2006, 2009; Chanson, Lubin, and Glockner, 2012). The method was robust and computationally inexpensive by generating a stochastic signal with prescribed mean velocity, Reynolds stresses, and time and length scale distributions. The prescribed input parameters were selected based upon the experimental results of the simulated flow conditions. The turbulent eddies were injected from the upstream end of the numerical domain and convected downstream.

Figure 3A shows the time variations of the longitudinal velocity component V_x of the initially steady flow before the generation of breaking bore with Fr = 1.5. The colored curves denoted instantaneous velocity at different vertical elevations z. The simulation was conducted for approximately 16 s (dimensionless time $t \times (g/d_1)^{1/2} \sim 121$), and the injected turbulence arrived at the probing point X = 9.6 m at approximately 2 s (dimensionless time $t \times (g/d_1)^{1/2} \sim 15$). The instantaneous longitudinal velocity demonstrated clearly some low-frequency fluctuations, with a period of oscillation of roughly between 3 and 4 s ($t \times (g/d_1)^{1/2} \sim 26$). The time-averaged longitudinal velocities at different vertical elevations were presented in Figure 3B. The numerical results were compared to experimental data of the same flow condition (EA_Fr1.5) and a 1/N power law (Figure 3B and 3C). The experimental results were collected using an acoustic Doppler velocimeter (ADV) at 200 Hz and then time-averaged over 30 s. The numerical results were time-averaged over 14 s, starting from the time at which turbulence arrived at the probing point. Using a cutoff frequent f_{cut} = 1 Hz, the low-pass filtered experimental time series (Figure 3C) showed close agreement with the numerical time series (Figure 3A) both qualitatively and quantitatively. Both experimental and numerical data highlighted larger oscillations in longitudinal velocity at lower vertical elevation ($z/d_1 \sim 0.06$), compared to higher vertical elevation ($z/d_1 \sim 0.8$). The period of large oscillation in velocity signal was similar for both numerical and experimental data.

The vertical profile of longitudinal velocity simulated by the numerical model showed a clear boundary layer, which was partially developed. The thickness of the numerical boundary layer was approximately 0.5 × d_1, which was comparable to the experimental finding. Within the boundary layer, the numerical data matched closely with the theoretical power law next the bed ($z/d_1 < 0.1$) and near the outer edge of the boundary layer (z/d_1 = 0.3–0.5). At the highest vertical elevation ($z/d_1 = 1$), the numerical data showed a large deviation from the experimental value, as well as the overall trend of the rest of the numerical data. Similar error at highest vertical elevation was also observed for steady flow with another flow condition (Figure 4B) and in previous findings by Simon (2014). Despite the highest vertical elevation, the numerical data showed a close agreement with the experimental data and theoretical curve for the rest of the vertical profile.

4.2. CFD simulation of the unsteady bore propagation

During the physical experiments, free-surface measurements were conducted non-intrusively using a series of acoustic displacement meters (ADMs), located at different longitudinal x locations along the channel centerline, where x is the distance from the channel's upstream end. The ADMs were calibrated against point gauge measurements before the experiments and sampled steady and unsteady flows at a sampling rate of 200 Hz. The physical experiments started with steady flows, running for at least 60 s before a downstream gate was rapidly closed, generating a tidal bore which propagated

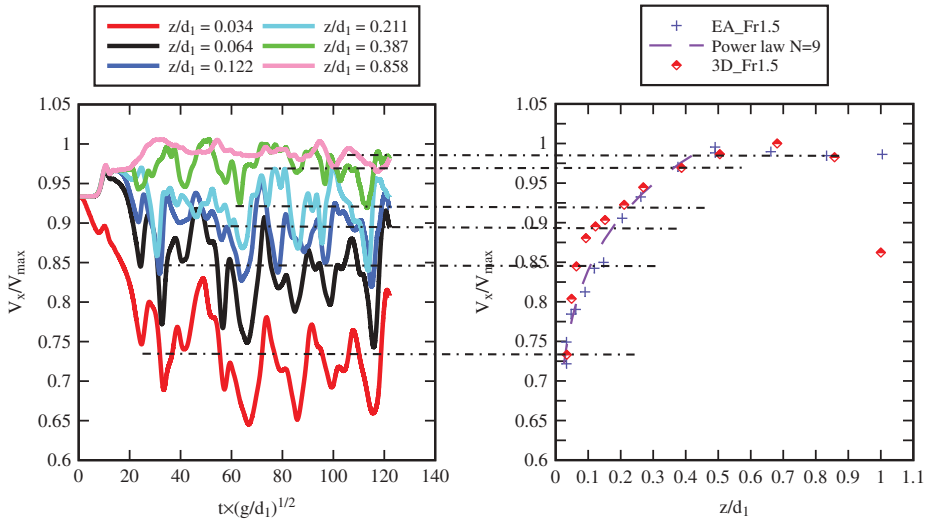

(A, Left) Time-variations of the instantaneous longitudinal velocity (CFD numerical 3D_Fr1.5)

(B, Right) Time-averaged vertical profile of the longitudinal velocity (CFD numerical, experimental and power law theoretical)

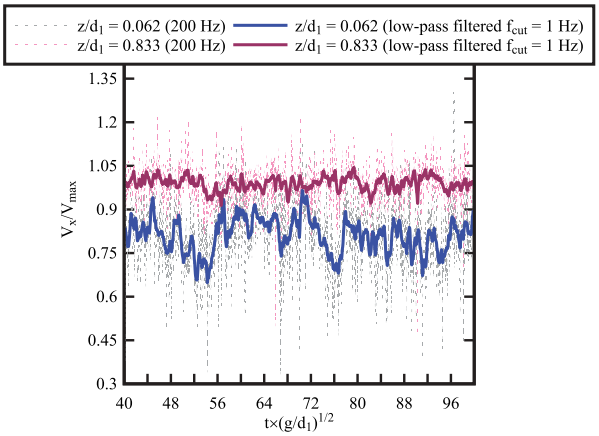

(C) Time-variations of the longitudinal velocity (experimental EA_Fr1.5): instantaneous data sampled at 200 Hz and low-pass filtered data using a cut-off frequency f_{cut} = 1 Hz

Figure 3. Time variations and time-averaged vertical profile of the longitudinal velocity component during the initially steady flow for breaking bore with Fr = 1.5; comparison between numerical, experimental, and theoretical results; numerical configuration 3D_Fr1.5; experimental configuration EA_Fr1.5.

upstream. The rapidly closing Tainter gate was located at downstream end (x = 18.1 m). Each experimental run was terminated after the bore traveled to the upstream intake. To perform ensemble-averaged measurements, at least 25 experimental runs were repeated for each flow condition listed in Table 3, and the results were ensemble-averaged.

The 2D unsteady numerical model started at the gate closure, i.e. initial condition t = 0 at gate closure, when tidal bores were generated. The simulation was stopped after the bore reached the inlet of numerical domain, and was considered one run. Due to limitation in computational time and capacity, each flow condition was only simulated for one run by the numerical CFD model. During the simulation, free-surface elevation was recorded at a number of longitudinal locations in the numerical channel. These locations were equivalent to the ADMs' locations in the physical channel. Figure 5 shows a comparison between the free-surface elevations varying with time as reproduced by the numerical model and measured by the experiments (ensemble-averaged and single run data). The flow condition shown by Figure 5 corresponded to tidal bores with the highest tested Froude number (Fr = 2.1), with the horizontal axis origin $t \times (g/d_1)^{1/2}$ = 0 at gate closure.

Close to the gate (Figure 6A), the free-surface showed an abrupt rise as the breaking bore was generated and propagated. Immediately upstream of the gate at x = 17.81 m, the free surface was modeled reasonably well by the numerical simulation. The timing of sudden increase in free surface, the gradient of

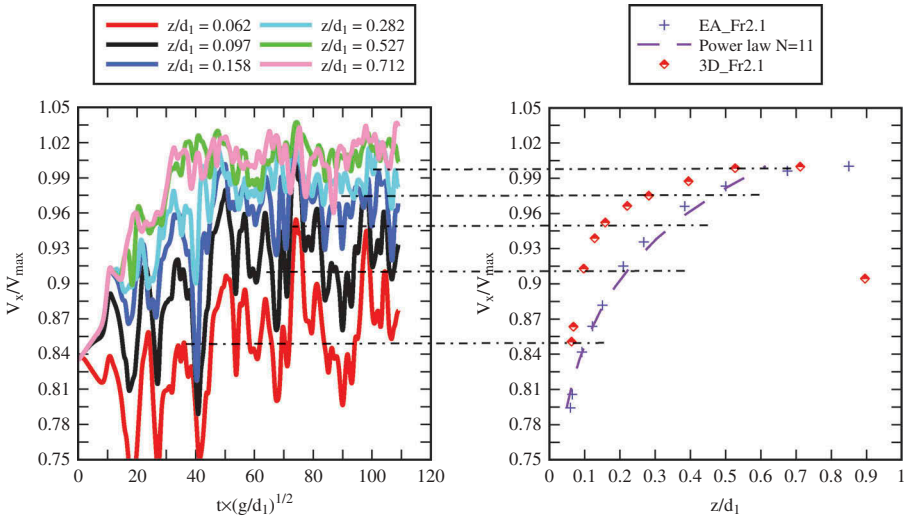

(A) Left: time-variations of the instantaneous longitudinal velocity (CFD numerical 3D_Fr2.1)

(B) Right: Time-averaged vertical profile of the longitudinal velocity (CFD numerical, experimental and power law theoretical)

Figure 4. Time variations and time-averaged vertical profile of the longitudinal velocity component during the initially steady flow for breaking bore with Fr = 2.1; comparison between numerical, experimental, and theoretical results; numerical configuration 3D_Fr2.1; experimental configuration EA_Fr2.1.

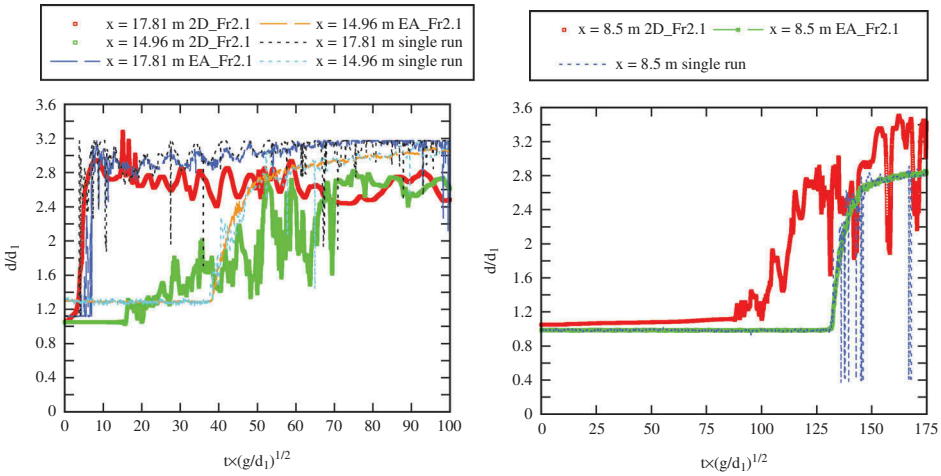

(A) Close to the gate

(B) Further upstream

Figure 5. Comparison of free-surface elevation variation with time between CFD numerical data, ensemble-averaged experimental data, and single-run experimental data at different longitudinal *x* positions (A) close to the gate and (B) further upstream; time $t = 0$ at gate closure; numerical configuration 2D_Fr2.1; experimental configuration EA_Fr2.1.

the increase and the maximum depth reached after were very similar, compared between numerical models and experimental data. After the first peak in depth, however, the numerical data started to decrease in depth and deviate from the experimental data. Further upstream at $x = 14.96$ m, the free-surface variations from the simulation and experiments showed some marked differences. The numerical depth started to increase much earlier compared to the experimental data, and showed jumps when increasing with time rather than a smooth continuous slope as seen in the experimental data. Although the peak in depth reached by the numerical data compared well in values to the experimental data, the trend of time variations after the peak was very different from the experimental results. Further upstream, the numerically simulated bore reached $x = 8.5$ m much earlier than the experimental observation. The time difference between the bore arrival time of the numerical and experimental results was approximately $\Delta t \times (g/d_1)^{1/2} = 28$, corresponding to a dimensional value of $\Delta t = 2.82$ s. The simulation of breaking bore with Fr = 1.5 showed similar lag in predicting the bore arrival time at upstream locations,

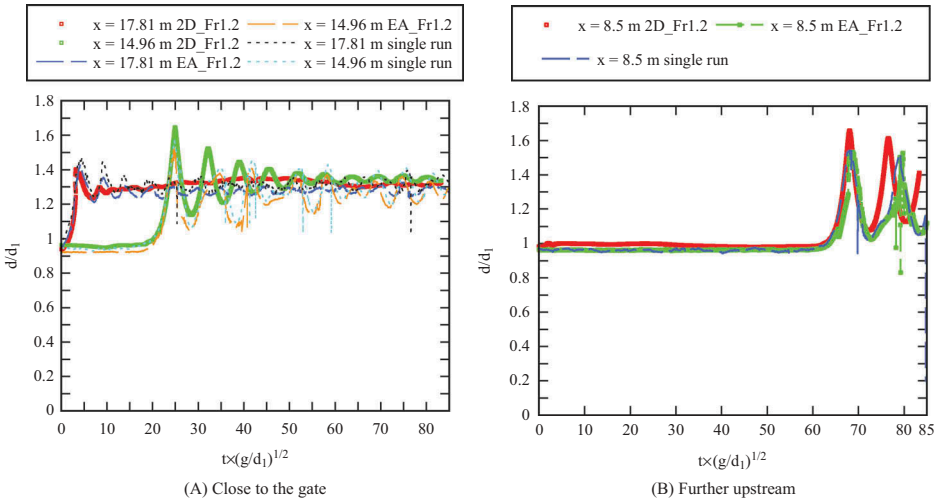

Figure 6. Comparison of free-surface elevation variation with time between CFD numerical data, ensemble-averaged experimental data, and single-run experimental data at different longitudinal x positions (A) close to the gate and (B) further upstream; time $t = 0$ at gate closure; numerical configuration 2D_Fr1.2; experimental configuration EA_Fr1.2.

compared to the experimental data. However, the lag was much smaller than 2D_Fr2.1 ($\Delta t \sim 0.6$ s for 2D_Fr1.5). Despite the time difference, the numerical data were similar to the experimental results at $x = 8.5$ m, with larger oscillations in depth as it turned to rise rapidly, and slightly overestimated the depth after the bore passage.

For undular bores with Fr = 1.2 (Figure 6), the numerical and experimental results showed close agreements in terms of the free-surface evolution with time near the gate and also further upstream ($x = 8.5$ m). The bore celerity was well modeled by the numerical simulation and almost no time lag was observed between the numerical and experimental data in terms of the bore arrival time, even further upstream at $x = 8.5$ m. As the undular bore propagated, the free-surface elevation increased smoothly with a train of secondary waves following the first wave front. The experimental data showed a decrease in wave height for the secondary undulations. This was also highlighted by the numerical data. The highest wave amplitude was associated with the bore front, namely the first wave crest immediately after the bore.

The numerical simulation showed an underestimation in the wave amplitude near the gate shortly after the generation ($x = 17.81$ m), however, tended to overestimation the amplitudes as the numerical bore traveled further upstream ($x = 14.96$ and 8.5 m). The numerical models were unable to reproduce the secondary waves with the same periodicity as the experimental model (Figure 6). The period of the secondary waves in the numerical simulation was much shorter than the experimental waves.

Overall, the free-surface variations with time modeled by the 2D simulation agreed very well with the experimental data close to the gate at generation, qualitatively and quantitatively. The height of the bore at generation tended to be lower for bores simulated numerically, as shown by results for all Froude numbers (Fr = 1.2, 1.5, and 2.1). As the bore propagated upstream, the numerical model tended to overestimate the bore celerity, resulted in early increase in depth at the same longitudinal location when compared to the experimental observation. This time difference in bore arriving time became more significant as the bore traveled further upstream, albeit less significant for small Froude number. In the 2D numerical simulation, velocity components in the longitudinal and vertical directions were recorded at $X = 9.6$ m in the numerical channel, equivalent to $x = 8.5$ m in the physical channel, and at a number of vertical elevations z. The unsteady turbulent velocity characteristics in the physical channel were measured using an ADV located at $x = 8.5$ m mid-channel. The ADV was equipped with a 3D side-looking head, capable of recording velocity components in the longitudinal, vertical, and transverse directions. The velocity measurements were conducted at different vertical elevations within the initially steady-flow depth. Experiments repeated 25 times for each flow condition and the results were ensemble-averaged. Velocity characteristics recorded by the numerical and physical models were compared for the same vertical elevation and flow condition. Figure 7 presents results for breaking bore with Fr = 2.1. Note that the velocity and depth data of the experimental results were synchronized manually with the numerical velocity data. The time $t = 0$ started at the numerical gate closure.

For all vertical elevations, the longitudinal velocity showed rapid deceleration associated with the bore passage, highlighted by both numerical and physical data (Figure 7A). The gradient of the deceleration was well predicted by the numerical model at all vertical elevations as compared to the experimental data. At the lowest vertical elevation ($z/d_1 = 0.1$), a longitudinal

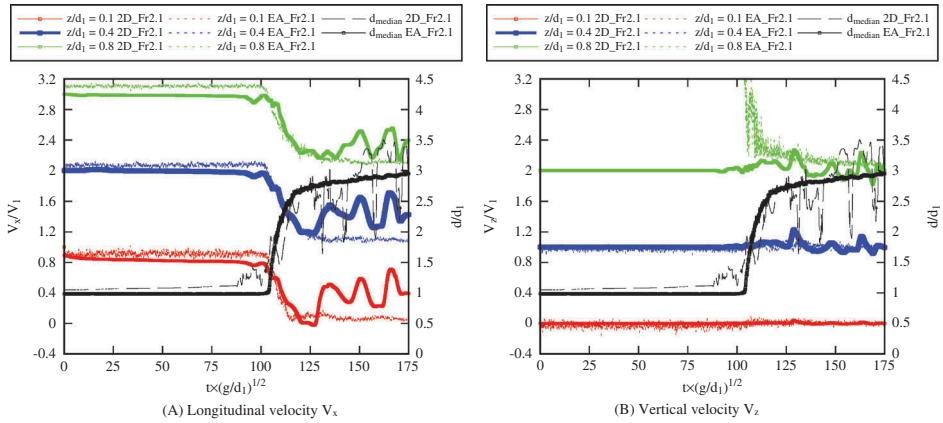

Figure 7. Comparison of velocity variation with time between CFD numerical data and ensemble-averaged experimental data for the (A) longitudinal velocity V_x and (B) vertical velocity V_z; time $t = 0$ at gate closure; velocity data offset by +1 every higher elevation; numerical configuration 2D_Fr2.1; experimental configuration EA_Fr2.1.

recirculation was observed in both numerical and physical data, marked by negative values reached at the end of the deceleration phase. The numerical recirculation occurred at a small time lag after the experimental recirculation. Nevertheless, the magnitudes of the two recirculation velocities were comparable. After the minimum value reached at the end of longitudinal deceleration, the velocity data measured by the physical experiments fluctuated around zero. The frequency of such fluctuations was relatively high ($f \sim 30$ Hz) and the magnitudes were low ($\sim 0.05 \times V_1$). On the other hand, the numerical data showed some large periodic oscillation in longitudinal velocity shortly after the end of the rapid deceleration. The period of the oscillation was as high as 1.6 s and the mean amplitude of such fluctuation was approximately $0.3 \times V_1$. This large periodic oscillation was considered not sensible, and possibly due to the constraint of the two dimensionality of the numerical model.

The vertical velocity showed an acceleration and then deceleration as the bore propagated (Figure 7B). The acceleration was more marked at higher vertical elevation near the free surface ($z/d_1 = 0.8$), with a maximum jump in velocity of $1.2 \times V_1$. The numerical data reproduced the vertical acceleration and deceleration, however, in a much less pronounced manner (maximum increase in velocity = $0.16 \times V_1$). This could be resulted from filtering the high-frequency fluctuations in LES, which smoothed out the very sharp acceleration and deceleration in velocity signals. After the bore passage, the mean vertical velocity of the numerical model, while showing some large periodic oscillation, was consistently lower than the magnitudes of the experimental data. At the two lower vertical elevations ($z/d_1 = 0.1$ and 0.4), the numerical model successfully simulated the mean vertical velocity before and after the bore passage that was quantitatively similar to the experimental value.

The numerical model showed a better comparison with the physical model for undular bores with Fr = 1.2 (Figure 8). At all vertical elevations, the longitudinal and vertical velocity data during the initially steady flow and rapid deceleration simulated numerically were quantitatively close to the experimental data. Difference in periodicity in the free-surface variations was observed

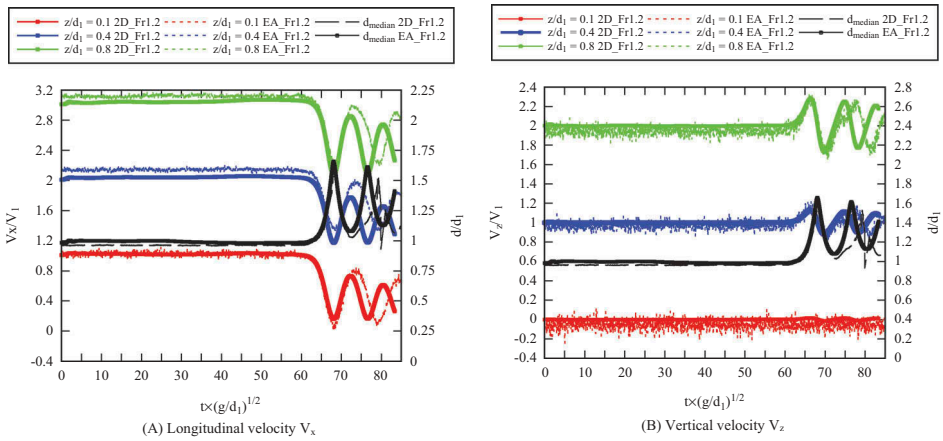

Figure 8. Comparison of velocity variation with time between CFD numerical data and ensemble-averaged experimental data for the (A) longitudinal velocity V_x and (B) vertical velocity V_z; time $t = 0$ at gate closure; velocity data offset by +1 every higher elevation; numerical configuration 2D_Fr1.2; experimental configuration EA_Fr1.2.

earlier in Figure 6. Herein, the periodicities in the oscillations of velocity data were also highlighted to be different between the two models. Nevertheless, the numerical model gave sound approximation in the time evolution of the 2D velocity characteristics in the steady flow and within the first wavelength of the unsteady flow at all vertical elevations within the inflow depth.

5. Final discussion

When comparing to previous CFD modeling attempts using Navier–Stokes equations, a number of specific features were observed. It was shown that, with identical initial flow conditions and boundary conditions, a small change in bore generation conditions (e.g. gate opening h_{out}) does not guarantee the validity of the new numerical results. In other words, a small change in bore conditions might require substantial changes in the numerical model parameters to achieve the same level of data quality/validation. The bore generation process by complete gate closure must be properly reproduced in the CFD model. This is a required, but not sufficient, condition. Further the (CFD) computation timescale is very different from the real timescale. For example, 1 s of real (physical) time might require more than 1 week of computation times on a super computer. In CFD modeling, the iteration time step is typically much shorter than the smallest sampling time increment. For example, some ADV sampling at 200 Hz means a sampling time increment of 5 ms.

Concerning laboratory physical modeling, the complete characterization of the turbulent processes necessitates to repeat experiments and to perform some ensemble-averaging. Great care is required to ensure (1) the repeatability of the experiments and (2) the synchronization between the repeated experiments. To date, only a few studies were able to conduct successfully experimental ensemble-averaging (Chanson and Docherty, 2012; Leng and Chanson, 2016a, 2017a, 2017b; Li and Chanson, 2017; Wang, Leng, and Chanson, 2017). More, construction details may vary from facilities to facilities, and flumes to flumes. Practical relevant details include the intake structure, the channel length, width, and rugosity. A 3D smooth convergent, located downstream of flow straighteners, produces the best inflow conditions. The length and width of the flume are other important experimental characteristics. If the flume is too short, the bore may not reach a quasi-steady-flow motion, while experiments in narrow flumes will be adversely affected by sidewall effects, leading to 3D flow motion. Boundary conditions are also a major concern, when trying to mimic experimental conditions. Even for a smooth channel, the floor and sidewalls are made of panels (e.g. 3.2 m long) with joints between panels. PVC floors can be connected very smoothly if carefully constructed (e.g. as at UQ), but sidewall joints can never be as smooth as the glass material. Any slight misalignment could induce local flow separation.

Initially, steady-flow conditions take several minutes to reach a quasi-stationary regime in a laboratory channel, contrarily to a CFD model. In laboratory, a tidal bore presents unique features for each run, implying the requirement for ensemble-averaged. Technically, (adverse) interactions between instruments could be experienced: ADV and ADV, ADV and ADV Profiler, array of ADV Profilers (Simon and Chanson, 2013; Leng and Chanson, 2016b, 2017c). Interactions between instruments and boundaries can also be source of problems (Koch and Chanson, 2005; Chanson, Trevethan, and Koch, 2007; Larrarte and Chanson, 2008). Most instrumentation (PIV, LDA, ADV) cannot record close to the free surface. A number of instruments (e.g. ADV) are adversely affected by the proximity of solid boundaries. Other instruments are affected the presence of bubbles in the bore roller, as well as suspended sediments in the water column. In laboratory, many instruments (e.g. Pitot, micro-propeller, ADV) are intrusive and their presence within the flow may affect adversely the flow field. This was partially discussed by Simon and Chanson (2013) and Leng and Chanson (2016b) in the context of positive surges and tidal bores. The experimental uncertainties must be carefully checked and documented. Any form of validation must account for the experimental errors, including instrumentation uncertainties, and human errors (e.g. operators). As many instruments deliver point measurements (e.g. Pitot, propeller, ADV, and LDA), this is also a major limitation and concern, when comparing laboratory and numerical results.

Field studies available in the literature are relatively scarce and detailed work is scarce. Performing measurements in the fluvial area is a real challenge. Indeed, in the published field studies, a number of problems were experienced. First of all, a main difficulty is finding an accessible measurement site for which logistics and deployment of acquisition instruments is possible on the desired duration. Secondly, the safety of people and the protection of equipment are a concern of every moment. A tidal bore is often described as being a very turbulent and energetic flow. The literature is full of anecdotes of material carried away, lost or destroyed (Mouaze, Chanson, and Simon, 2010; Reungoat, Chanson, and Caplain, 2012; CHANSON and LUBIN, 2013). We can also mention historical stories or recent news about accidental drownings of walkers or sailors, e.g. in China (Pan and Chanson, 2015). Moreover, all field studies are dependent on the conditions under which the work is carried out, including climatic events (rain and wind conditions) or floods (Reungoat, Chanson, and Caplain, 2014), sometimes complicating the experimenters' task or making the phenomenon unobservable. Many technical limitations are also to be deplored. It is

extremely rare to have all the desired instrumentation, or even to be able to deploy it. It often happens that the expected information is also incomplete (breakdowns, interruptions of measurements, etc.).

It is obviously extremely complicated, if not impossible, to access detailed information at all spatiotemporal scales during the propagation of a real tidal bore over long distances in nature. We have thus devoted our work to the reproduction of laboratory experiments. However, the first experiments of intensive numerical simulations dedicated to breaking waves allow us to consider future realizations of simulations of tidal bore in real conditions.

As Keylock et al. (2005) who analyzed the potential applications of the LES to some problems of fluvial geomorphology, the numerical simulation offers a large interest in accessing a lot of information. In the case of irregular and highly variable bathymetries, zones of different roughness, configurations involving meanders or confluences, obstacles, or hydraulic structures, numerical simulation provides information on the dynamics of large scales and their impact on suspension and sediment mixing. Examples of using Navier–Stokes codes can be found for the study of flow in fluvial flows in large numerical domains (Keylock, Constantinescu, and Hardy, 2012). Kang et al. (2011) simulated the flow in a large experimental basin (50 m long, 2 m wide, and 0.1 m deep), discretized by 67 million mesh grid points and using 160 processors. The results showed a good agreement with experimental measurements. These encouraging results confirm the potential of our numerical methods to access the complex structure of the flow in terms of primary and secondary vortices in the curved areas of the channels.

Real configurations are within the reach of modern supercomputers. In future works, special attention will be given to the interaction between the tidal bore and structures such as piles of pontoons, rocks, or built docks, which undergo considerable efforts during the passage of tides and around which large areas of scour and erosion are observed. The stability of the banks is also a problem to take into account. More dramatically, the overflows tidal storms can cause many human casualties, such as during the annual festivities in Hangzou, China. Numerical simulations can be utilized at the service of studies in order to anticipate accidents (definition of zones forbidden to the public, evaluation of effectiveness of protections, etc.).

On the basis of our work on tidal bores, tsunami penetration and retreat in rivers can be considered for analogy (Chanson and Lubin, 2013). A current challenge is to try to improve the prediction of floods generated by tsunamis breaking on the coast, entering rivers and in the land over very long distances. Numerous studies have demonstrated the importance of tsunami penetration in rivers (several tens of kilometers). The floods have been aggravated by this natural path of propagation, and therefore the damage and loss of lives. However, it is not easy to imagine systems for protecting rivers and their banks, without altering their main function which is to link land and ocean, or unbalance the interactions between rivers/estuaries/ocean. So we could use our results as an analogy to participate in this research effort. In the same way as for river flows, simulating the 3D Navier–Stokes equations can provide access to the details of the flow generated by tsunamis submerging a coastal zone. In particular, it will be interesting to simulate mitigation of tsunami propagation by coastal vegetation or interactions with habitats (study of building resistance, better management of land use, etc.). A very recent study showed the path for future detailed studies in complicated channel geometries (Kiri, Leng, and Chanson, 2017).

In summary, the development and validation of CFD numerical models are not trivial. This requires some fundamental understanding of the numerical model and its limitations, as well as some in-depth knowledge of the physical model, its characteristics, and its instrumentation. The latter is critical to ensure the suitability of the experimental modeling data for CFD validation, as not all experimental setups are truly equal. The present experience suggested that a proper CFD modeling validation necessitates a team of researchers with both numerical and physical expertise. Ultimately both numerical and physical models are developed to reproduce a complicated 3D unsteady geophysical phenomenon, i.e. a tidal bore: "*Validation has highest priority* [...] *because Nature is the final jury*" (Roache, 1998).

Acknowledgments

The financial support through the Agence Nationale de la Recherche (Project MASCARET ANR-10-BLAN-0911) and the School of Civil Engineering at the University of Queensland is acknowledged. The first and third authors acknowledge some traveling grant from the UQ Graduate School (GSITA). This work was granted access to the HPC (High Performan Computing) resources of CINES (Centre Informatique National de l'Enseignement Supérieur), under the allocation A0032A06104 made by GENCI (Grand Equipement National de Calcul Intensif). Computer time for this study was also provided by the computing facilities at MCIA (Mésocentre de Calcul Intensif Aquitain) of the Université de Bordeaux and of the Université de Pau et des Pays de l'Adour.

Disclosure Statement

No potential conflict of interest was reported by the authors.

Funding

The financial support through the Agence Nationale de la Recherche (Project MASCARET ANR-10-BLAN-0911) and the School of Civil Engineering at the University of Queensland is acknowledged. The first and third authors acknowledge some traveling grant from the UQ Graduate School (GSITA).

ORCID

Xinqian Leng http://orcid.org/0000-0001-8472-7925
Bruno Simon http://orcid.org/0000-0002-6596-0905
Pierre Lubin http://orcid.org/0000-0003-1957-6854
Hubert Chanson http://orcid.org/0000-0002-2016-9650

References

Chanson, H. 2009. "Current Knowledge in Hydraulic Jumps and Related Phenomena. A Survey of Experimental Results." *European Journal of Mechanics B/ Fluids* 28 (2): 191–210. doi:10.1016/j.euromechflu.2008.06.004).

Chanson, H. 2010. "Undular Tidal Bores: Basic Theory and Free-Surface Characteristics." *Journal of Hydraulic Engineering, ASCE* 136 (11): 940–944. doi:10.1061/(ASCE)HY.1943-7900.0000264).

Chanson, H. 2012. "Momentum Considerations in Hydraulic Jumps and Bores." *Journal of Irrigation and Drainage Engineering, ASCE* 138 (4): 382–385. doi:10.1061/(ASCE)IR.1943-4774.0000409).

Chanson, H., P. Lubin, and S. Glockner. 2012. "Unsteady Turbulence in a Shock: Physical and Numerical Modelling in Tidal Bores and Hydraulic Jumps." In *Turbulence: Theory, Types, and Simulation*, edited by R. J. Marcuso, 113–148. Vol. 3. Hauppauge, N.Y: Nova Science Publishers.

Chanson, H. 2013. "Hydraulics of Aerated Flows: Qui Pro Quo?" *Journal of Hydraulic Research* 51(3):223–243. IAHR, Invited Vision paper. doi:10.1080/00221686.2013.795917).

Chanson, H. 2016. "Atmospheric Noise of a Breaking Tidal Bore." *Journal of the Acoustical Society of America* 139 (1): 12–20. doi:10.1121/1.4939113).

Chanson, H., D. Reungoat, B. Simon, and P. Lubin. 2011. "High-Frequency Turbulence and Suspended Sediment Concentration Measurements in the Garonne River Tidal Bore." *Estuarine Coastal and Shelf Science* 95 (2–3): 298–306. doi:10.1016/j.ecss.2011.09.012).

Chanson, H., M. Trevethan, and C. Koch. 2007. "Turbulence Measurements with Acoustic Doppler Velocimeters. Discussion." *Journal of Hydraulic Engineering* ASCE. 133 (11): 1283–1286. doi:10.1061/(ASCE)0733-9429(2005)131:12(1062)). (ISSN 0733-9429).

Chanson, H., and N. J. Docherty. 2012. "Turbulent Velocity Measurements in Open Channel Bores." *European Journal of Mechanics B/Fluids* 32: 52–58. doi:10.1016/j.euromechflu.2011.10.001).

Chanson, H., and P. Lubin. 2013. "Chapter 3: Mixingand Sediment Processes induced by Tsunamis propagating Upriver". In Tsunamis: Economic Impact, Disaster Management and Future Challenges, edited by T. Cai, Series of Natural Disaster Research, Prediction and Mitigation, Nova Science Publishers, pp 65-102.

Cunge, J. A. 1966. "Comparaison Des Résultats Des Essais d'Intumescences Effectués Sur Le Modèle Réduit Et Sur Le Modèle Mathématique Du Canal Oraison-Manosque." *Journal La Houille Blanche* 1: 55–69 & 79. ('Comparison of Positive Surge Results between Physical Modelling and Numerical Modelling of the Oraison-Manosque Canal.'). (In French). doi:10.1051/lhb/1966003.

Faas, R. W. (1995). "Rheological Constraints on Fine Sediment Distribution and Behavior: The Cornwallis Estuary, Novia Scotia." *Proceedings of Canadian Coastal Conference*, Dartmouth, Nova Scotia, pp. 301–314.

Jarrin, N., R. Prosser, J. C. Uribe, S. Benhamadouche, and D. Laurence. 2009. "Reconstruction of Turbulent Fluctuations for Hybrid RANS/LES Simulations Using a Synthetic-Eddy Method." *Proceedings of 7th International Symposium on Engineering Turbulence Modelling and Measurements, ETMM7* 30 (3): 435–442.

Jarrin, N., S. Benhamadouche, D. Laurence, and R. Prosser. 2006. "A Synthetic-Eddy Method for Generating Inflow Conditions for Large-Eddy Simulations." *International Journal of Heat and Fluid Flow* 27 (4): 585–593. doi:10.1016/j.ijheatfluidflow.2006.02.006.

Kang, S., A. Lightbody, C. Hill, and F. Sotiropoulos. 2011. "High-Resolution Numerical Simulation of Turbulence in Natural Waterways." *Advances in Water Resources* 34: 98–113. doi:10.1016/j.advwatres.2010.09.018.

Keevil, C. E., H. Chanson, and D. Reungoat. 2015. "Fluid Flow and Sediment Entrainment in the Garonne River Bore and Tidal Bore Collision." *Earth Surface Processes and Landforms* 40 (12): 1574–1586. doi:10.1002/esp.3735).

Keylock, C. J., G. Constantinescu, and R. J. Hardy. 2012. "The Application of Computational Fluid Dynamics to Natural River Channels: Eddy Resolving versus Mean Flow Approaches." *Geomorphology* 179: 1–20. doi:10.1016/j.geomorph.2012.09.006.

Keylock, C. J., R. J. Hardy, D. R. Parsons, R. I. Ferguson, S. N. Lane, and K. S. Richards. 2005. "The Theoretical Foundations and Potential for Large-Eddy Simulation (LES) in Fluvial Geomorphic and Sedimentological Research." *Earth-Science Reviews* 71: 271–304. doi:10.1016/j.earscirev.2005.03.001.

Khezri, N. (2014). "Modelling Turbulent Mixing and Sediment Process beneath Tidal Bores: Physical and Numerical Investigations." *Ph.D. thesis*, School of Civil Engineering, The University of Queensland, Brisbane, Australia, 267 pp.

Kiri, U., X. Leng, and H. Chanson (2017). "Positive Surge Propagation in Non-Rectangular Channels." Proceedings of 13th Hydraulics in Water Engineering Conference HIWE2017, Engineers Australia, Sydney, 13-16 Nov, 9 pages (ISBN 78-1-925627-03-9) .

Koch, C., and H. Chanson (2005). "An Experimental Study of Tidal Bores and Positive Surges: Hydrodynamics and Turbulence of the Bore Front." *Report No. CH56/05*, Dept. of Civil Engineering, The University of Queensland, Brisbane, Australia, Jul, 170 1864998245.

Koch, C., and H. Chanson. 2009. "Turbulence Measurements in Positive Surges and Bores." *Journal of Hydraulic Research, IAHR* 47 (1): 29–40. doi:10.3826/jhr.2009.2954).

Larrarte, F., and H. Chanson (2008). "Experiences and Challenges in Sewers: Measurements and Hydrodynamics." *Proceedings of the International Meeting on Measurements and Hydraulics of Sewers IMMHS'08*, Summer School GEMCEA/LCPC, 19-21 Aug 2008, Bouguenais, Hydraulic Model Report No. CH70/08, Div. of Civil Engineering, The University of Queensland, Brisbane, Australia, 114 (ISBN 9781864999280).

Leng, X., and H. Chanson. 2015a. "Breaking Bore: Physical Observations of Roller Characteristics." *Mechanics Research Communications* 65: 24–29. doi:10.1016/j.mechrescom.2015.02.008).

Leng, X., and H. Chanson. 2015b. "Turbulent Advances of a Breaking Bore: Preliminary Physical Experiments."

Experimental Thermal and Fluid Science 62: 70–77. doi:10.1016/j.expthermflusci.2014.12.002).

Leng, X., and H. Chanson. 2016a. "Coupling between Free-Surface Fluctuations, Velocity Fluctuations and Turbulent Reynolds Stresses during the Upstream Propagation of Positive Surges, Bores and Compression Waves." *Environmental Fluid Mechanics* 16 (4): 695–719. and digital appendix. doi:10.1007/s10652-015-9438-8.

Leng, X., and H. Chanson (2016b). "Unsteady Turbulent Velocity Profiling in Open Channel Flows and Tidal Bores Using a Vectrino Profiler." *Hydraulic Model Report No. CH101/15*, School of Civil Engineering, The University of Queensland, Brisbane, Australia, 118 pp (ISBN 978-1-74272-145-3).

Leng, X., and H. Chanson. 2017a. "Upstream Propagation of Surges and Bores: Free-Surface Observations." *Coastal Engineering Journal* 59 (1): paper 1750003, 32 pages & 4 videos. doi:10.1142/S0578563417500036).

Leng, X., and H. Chanson. 2017b. "Integral Turbulent Scales in Unsteady Rapidly Varied Open Channel Flows." *Experimental Thermal and Fluid Science* 81: 382–395. doi:10.1016/j.expthermflusci.2016.09.017).

Leng, X., and H. Chanson. 2017c. "Unsteady Velocity Profiling in Bores and Positive Surges." *Flow Measurement and Instrumentation* 54: 136–145. doi:10.1016/j.flowmeasinst.2017.01.004).

Li, Y., and H. Chanson (2017). "Free-Surface and Velocity Characteristics of Tidal Bore Propagation against a Slope: Experiments on Decelerating Bores." *Proc. 37th IAHR World Congress*, Kuala Lumpur, Malaysia, 13-18 Aug, 10 .

Lighthill, J. 1978. *Waves in Fluids*, 504. Cambridge, UK: Cambridge University Press.

Lubin, P., and H. Chanson. 2017. "Are Breaking Waves, Bores, Surges and Jumps the Same Flow?" *Environmental Fluid Mechanics* 17 (1): 47–77. doi:10.1007/s10652-016-9475-y).

Lubin, P., S. Glockner, and H. Chanson. 2010a. "Numerical Simulation of a Weak Breaking Tidal Bore." *Mechanics Research Communications* 37 (1): 119–121. doi:10.1016/j.mechrescom.2009.09.008).

Lubin, P., H. Chanson, and S. Glockner. 2010b. "Large Eddy Simulation of Turbulence Generated by a Weak Breaking Tidal Bore." *Environmental Fluid Mechanics* 10 (5): 587–602. doi:10.1007/s10652-009-9165-0).

Lubin, P., and S. Glockner. 2015. "Numerical Simulations of Three-Dimensional Plunging Breaking Waves: Generation and Evolution of Aerated Vortex Filaments." *Journal of Fluid Mechanics* 767: 364–393. doi:10.1017/jfm.2015.62).

Madsen, P. A., H. J. Simonsen, and C. H. Pan. 2005. "Numerical Simulation of Tidal Bores and Hydraulic Jumps." *Coastal Engineering* 52: 409–433. doi:10.1016/j.coastaleng.2004.12.007).

Mouaze, D., H. Chanson, and B. Simon (2010). "Field Measurements in the Tidal Bore of the Sélune River in the Bay of Mont Saint Michel (September 2010)." Hydraulic Model Report No. CH81/10, School of Civil Engineering, University of Queensland, Brisbane, Australia, 72 (ISBN 9781742720210).

Pan, D. Z., and H. Chanson (2015). "Physical Modelling of Tidal Bore Dyke Overtopping: Implication on Individuals' Safety." *Proc. 36th IAHR World Congress*, The Hague, The Netherlands, 27 Jun-3 Jul, Theme 4, pp. 3824–3831.

Peregrine, D. H. 1966. "Calculations of the Development of an Undular Bore." *Journal of Fluid Mechanics* 25: 321–330. doi:10.1017/S0022112066001678.

Ponsy, J., and M. Carbonnell (1966). "Etude Photogrammétrique d'Intumescences Dans Le Canal De l'Usine d'Oraison (Basses-Alpes)." ('Photogrammetric Study of Positive Surges in the Oraison Powerplant Canal.') Jl Soc. Française de Photogram., Vol. 22, pp. 18–28 (in French).

Preissmann, A., and J. A. Cunge. 1967. "Low-Amplitude Undulating Hydraulic Jump In Trapezoidal." *Journal of Hydraulic Research, IAHR* 5 (4): 263–279. doi:10.1080/00221686709500211.

Reungoat, D., H. Chanson, and B. Caplain (2012). "Field Measurements in the Tidal Bore of the Garonne River at Arcins (June 2012)." Hydraulic Model Report No. CH89/12, School of Civil Engineering, The University of Queensland, Brisbane, Australia, 121 (ISBN 9781742720616).

Reungoat, D., H. Chanson, and B. Caplain. 2014. "Sediment Processes and Flow Reversal in the Undular Tidal Bore of the Garonne River (France)." *Environmental Fluid Mechanics* 14 (3): 591–616. doi:10.1007/s10652-013-9319-y).

Roache, R. L. 1998. "Verification of Codes and Calculations." *AIAA Journal* 36 (5): 696–702. doi:10.2514/2.457.

Simon, B. (2014). "Effects of Tidal Bores on Turbulent Mixing: A Numerical and Physical Study in Positive Surges." *Ph.D. thesis*, School of Civil Engineering, The University of Queensland, Brisbane, Australia, 259 pp and 7 movies (DOI: 10.14264/uql.2014.19).

Simon, B., and H. Chanson (2013). "Turbulence Measurements in Tidal Bore-Like Positive Surges over a Rough Bed." *Hydraulic Model Report No. CH90/12*, School of Civil Engineering, The University of Queensland, Brisbane, Australia, 176 (ISBN 9781742720685).

Wang, H., X. Leng, and H. Chanson (2017). "Bores and Hydraulic Jumps. Environmental and Geophysical Applications." *Engineering and Computational Mechanics*, Proceedings of the Institution of Civil Engineers, UK, 170 (EM1), 25–42 (DOI:10.1680/jencm.16.00025).